

Motion of a thin elliptic plate under symmetric and asymmetric orthotropic friction forces.

O. A. Silantyeva¹, N. N. Dmitriev

*Department of Mathematics and Mechanics, Saint-Petersburg State University
198504 Universitetski pr.28, Peterhof, Saint-Petersburg, Russia*

Abstract

Anisotropy of friction force is proved to be an important factor in various contact problems. We study dynamical behavior of thin plates with respect to symmetric and asymmetric orthotropic friction. Terminal motion of plates with circular and elliptic contact areas is mainly analyzed. Evaluation of friction forces for both symmetric and asymmetric orthotropic cases are shown. Regular pressure distribution is considered. Differential equations are formulated and solved numerically for a number of initial conditions. Examples show significant influence of friction force asymmetry on the motion.

Keywords: Anisotropic friction, Orthotropic friction, Asymmetric friction, Elliptic contact area, Terminal motion

1 Introduction

Anisotropy of friction force is an important factor in contact problems. Surfaces of wide number of materials (crystals, composites, polymers, wood) are anisotropic due to their internal properties. Engineering materials usually are manufactured in the way that oriented surface roughness textures appear. Smart materials with directional asymmetry are developed [3]. Using atomic force microscope (AFM) in [5] way of obtaining frictional hodographs is shown. This information is related to intensity and symmetry of friction phenomenon. Contact process with wear, deformation, surface evolution, thermal and chemical variations, impact frictional behavior of materials. A review [24] discusses factors influencing friction forces and approaches of friction force modeling. The paper [25] presents examples of friction forces with respect to contact stresses calculation in various computational tasks.

Influence of anisotropy at contact interface has been widely investigated experimentally and theoretically during last decades by [7, 13, 15, 21] and others. Examples of centrosymmetric and non-centrosymmetric friction are presented in [23].

¹Corresponding author E-mail: olga.silantyeva@gmail.com

In [1] authors proposed a generalized Coulomb-like friction law and set up a series of experiments with parallelepiped test specimens with asymmetric surface texture.

This study deals with symmetric and asymmetric orthotropic friction. We investigate dynamical behavior of sliding and spinning disks on anisotropic surfaces. In [21] some experimental and theoretical results regarding terminal motion of sliding spinning disks are presented. Sliding and spinning motions are also considered in [13]. However, both papers assume isotropic friction force. We attempt to finalize our work done during last years. We investigated a circular area with symmetric orthotropic friction and uniform pressure distribution in [8], an elliptic area with symmetric orthotropic friction and uniform pressure distribution in [12] and linear pressure distribution in [11], a mass point with asymmetric friction in [9], a mass point and elliptic plate with asymmetric friction in [20] and a ring with asymmetric friction in [10].

In the paper we present descriptions, regarding the developed theory for circular and elliptic thin plates under uniform pressure distribution. Effect of asymmetry of friction force is taken into account and compared with symmetric case. Asymmetry of friction is used in omni-directional vehicles [14] and robotics [6]. Elliptical contact area, which appear in railway problems (see [18]), in multi-body dynamics during analysis of foot motion (see [16]) and other situations is considered. All equations are evolved for this contact domain as a generalized form which include circular area as a test base. Main results are presented for the elliptic contact area.

2 Formulation of the problem

2.1 Friction law

Let us consider terminal motion of a thin plate on a horizontal plane with anisotropic friction force. Anisotropic friction force \mathbf{T} at a point M of a moving body according to [22] can be written in the following form:

$$\mathbf{T} = -p_M \mathcal{F}(M) \frac{\mathbf{v}}{|\mathbf{v}|}, \quad \mathcal{F}(M) = \begin{pmatrix} f_x & f \\ -f & f_y \end{pmatrix}, \quad (1)$$

here p_M is a normal pressure at the point M , $\mathcal{F}(M)$ is a friction matrix written with respect to a stationary coordinate system Oxy (see [7]), \mathbf{v} is a velocity vector of the point M .

Friction is *symmetric orthotropic* in case the friction matrix $\mathcal{F}(M)$ is a tensor which components are constant and do not depend on the orientation of contacting

areas. This approximation is possible for the case when hardness of one plane is greater than hardness of another one or one of the contact bodies has isotropic frictional properties. If hardness of each material of the contacting pair is similar we should use a more complicated law for friction force (see [7]).

Friction is *asymmetric orthotropic* if in the friction matrix components differ in negative and positive directions of sliding with $f_{x+} \geq f_{x-}$, $f_{y+} \geq f_{y-}$. Thus, in (1) we have:

$$f_x = \begin{cases} f_{x+}, & v_x \geq 0 \\ f_{x-}, & v_x < 0 \end{cases} \quad \text{and} \quad f_y = \begin{cases} f_{y+}, & v_y \geq 0 \\ f_{y-}, & v_y < 0 \end{cases},$$

here v_x, v_y are projections of velocity vector in Oxy .

For both cases term *orthotropic* means an assumption that $f = 0$.

2.2 Equations of motion

Let us introduce a moving coordinate system $C\xi\eta\zeta$, associated with the plate. For the elliptic plate this coordinate system is associated with the principal axes of it. Axis $C\zeta$ is perpendicular to the plane of sliding. Stationary coordinate system Oxy is selected thus, that the friction matrix has the form (1) and axes Ox and Oy are in the sliding plane. Let φ be an angle between Ox and $C\xi$, ϑ is an angle between axis Ox and \mathbf{v}_C which is a velocity of a center of mass of the plate.

$$\mathbf{v}_C = v_C(\cos \vartheta \mathbf{i} + \sin \vartheta \mathbf{j}), \quad (2)$$

where v_C is a velocity value, \mathbf{i} , \mathbf{j} are unit vectors of axes Ox , Oy . Vector of an angular velocity is $\boldsymbol{\omega} = \omega \mathbf{k}$, where $\omega = \dot{\varphi}$, \mathbf{k} is a unit vector of axis Oz .

Euler equation $\mathbf{v}_M = \mathbf{v}_C + \boldsymbol{\omega} \times \mathbf{CM}$ allows us to write the following statements:

$$\begin{aligned} v_x &= v_C \cos \vartheta - \omega y', & v_y &= v_C \sin \vartheta + \omega x', \\ x' &= \xi \cos \varphi - \eta \sin \varphi, & y' &= \xi \sin \varphi + \eta \cos \varphi, \\ h &= \eta \cos(\vartheta - \varphi) - \xi \sin(\vartheta - \varphi), \\ v_M &= \sqrt{v_C^2 + \omega^2(\xi^2 + \eta^2) - 2v_C\omega h}. \end{aligned} \quad (3)$$

With the anisotropic friction law (1) and equations (3) we can write projections of the total friction force vector \mathbf{T} and the total friction moment \mathbf{M} in the form:

$$\begin{aligned} T_x &= \iint_{\Omega} \tau_x d\xi d\eta, & T_y &= \iint_{\Omega} \tau_y d\xi d\eta, \\ M_{C\zeta} &= \iint_{\Omega} (\tau_y x' - \tau_x y') d\xi d\eta, \\ \tau_x &= -f_x p(\xi, \eta) \frac{v_x(\xi, \eta)}{v_M(\xi, \eta)}, & \tau_y &= -f_y p(\xi, \eta) \frac{v_y(\xi, \eta)}{v_M(\xi, \eta)}, \end{aligned} \quad (4)$$

where Ω is an integration area.

Equations of motion in the Frenet-Serret frame with respect to (4) are as follows:

$$\begin{aligned} m\dot{v}_C &= T_\tau = T_x \cos \vartheta + T_y \sin \vartheta, \\ m v_C \dot{\vartheta} &= T_n = -T_x \sin \vartheta + T_y \cos \vartheta, \\ I\dot{\omega} &= M_{C\zeta}, \end{aligned} \quad (5)$$

where m is a mass of the plate, I is a plate's inertia moment about $C\zeta$, T_τ and T_n are projections of a friction force vector \mathbf{T} on tangential and normal axes respectively, $M_{C\zeta}$ is a friction moment about axis $C\zeta$.

Let's rewrite the system (5) in the dimensionless form using following relations:

$$\begin{aligned} I &= m a^2 I^*, \quad \xi = a \xi^*, \quad \eta = a \eta^*, \quad v_C = v_C^* \sqrt{a g}, \\ \omega &= \omega^* \sqrt{\frac{g}{a}}, \quad t = t^* \sqrt{\frac{a}{g}}, \quad \vartheta = \frac{d\vartheta}{dt^*} \sqrt{\frac{g}{a}}, \quad p = p^* \frac{m g}{S} \end{aligned}$$

and let's introduce a variable $\beta = \frac{v_C}{\omega} = a \beta^*$ and a parameter $\mu = f_y - f_x$. In these equations parameter a is measurable, it is the length of the largest line from point C to the area's boundary, S is a contact area.

Equations (5) in dimensionless form (asterisks are omitted):

$$\begin{aligned} \frac{dv_C}{dt} &= - \iint_{\Omega} p(\xi, \eta) \left[\frac{\beta(f_x + \mu \sin^2 \vartheta) + f_x s_1 + \mu s_3 + f s_2}{s} \right] d\xi d\eta, \\ v_C \frac{d\vartheta}{dt} &= - \iint_{\Omega} p(\xi, \eta) \left[\frac{\beta(\mu \sin \vartheta \cos \vartheta - f) + f_x s_2 + \mu s_4 - f s_1}{s} \right] d\xi d\eta, \quad (6) \\ \frac{d\omega}{dt} &= - \iint_{\Omega} \frac{p(\xi, \eta)}{I} \left[\frac{\beta(f_x s_1 + \mu s_3 - f s_2) + f_x(\xi^2 + \eta^2) + \mu s_0^2}{s} \right] d\xi d\eta, \end{aligned}$$

where

$$\begin{aligned} s &= \sqrt{\beta^2 + \xi^2 + \eta^2 + 2\beta s_1}, \quad s_0 = \xi \cos \varphi - \eta \sin \varphi, \\ s_1 &= \xi \sin(\vartheta - \varphi) - \eta \cos(\vartheta - \varphi), \quad s_2 = \xi \cos(\vartheta - \varphi) + \eta \sin(\vartheta - \varphi), \\ s_3 &= \xi \cos \varphi \sin \vartheta - \eta \sin \varphi \sin \vartheta, \quad s_4 = \xi \cos \varphi \cos \vartheta - \eta \sin \varphi \cos \vartheta. \end{aligned}$$

System of equations (6) is general. It is possible to numerically evaluate this system directly. However, in most cases it is better to integrate forces in the right part of the system at least once – it accelerates calculations and simplifies analysis. We will study later uniform pressure distribution and only orthotropic case.

3 Friction force evaluation

3.1 Symmetric orthotropic friction

We will evaluate friction forces using method developed by A.I. Lurye in [17]. Let us introduce polar coordinate system, which origin is in the instantaneous velocity center G , polar axis is a ray from simultaneous velocity center through plate center C , γ is a polar angle. We will differ two cases of simultaneous velocity center position: inside and outside area, covered by plate, see figure 1.

Velocity vector is the following:

$$\mathbf{v} = v(\cos(\vartheta + \gamma)\mathbf{i} + \sin(\vartheta + \gamma)\mathbf{j}),$$

where v is a velocity value, \mathbf{i}, \mathbf{j} are unit vectors of coordinate system axes.

Vector of elementary friction force is:

$$\boldsymbol{\tau} = -p(f_x \cos(\vartheta + \gamma)\mathbf{i} + f_y \sin(\vartheta + \gamma)\mathbf{j}). \quad (7)$$

Friction force and moment taking into account (7) in stationary coordinate system are the following:

$$\begin{aligned} T_x &= -pf_x \int_{\gamma_1}^{\gamma_2} \int_{r_1(\gamma)}^{r_2(\gamma)} \cos(\vartheta + \gamma) r dr d\gamma, \\ T_y &= -pf_y \int_{\gamma_1}^{\gamma_2} \int_{r_1(\gamma)}^{r_2(\gamma)} \sin(\vartheta + \gamma) r dr d\gamma, \\ M_G &= -p \int_{\gamma_1}^{\gamma_2} \int_{r_1(\gamma)}^{r_2(\gamma)} (f_x + \frac{\mu}{2} - \frac{\mu}{2} \cos(2\vartheta + 2\gamma)) r^2 dr d\gamma, \\ M_C &= M_G - CG \cdot p \int_{\gamma_1}^{\gamma_2} \int_{r_1(\gamma)}^{r_2(\gamma)} (\frac{\mu}{2} \cos(\gamma) - \frac{\mu}{2} \cos(2\vartheta + \gamma) + f_x \cos(\gamma)) r dr d\gamma. \end{aligned} \quad (8)$$

We assume that the plate has elliptical shape with semi-axes a and b , where a is a major semi-axis, than

$$m = \rho \pi ab, \quad \kappa = \sqrt{1 - e^2}, \quad I = \frac{\rho \pi \kappa a^4 (1 + \kappa^2)}{4}, \quad p = \frac{mg}{\pi ab},$$

where m is a mass of the plate, ρ is a mass density of the plate, e is an ellipse eccentricity, p is a value of uniformly distributed pressure, g is the acceleration of free fall.

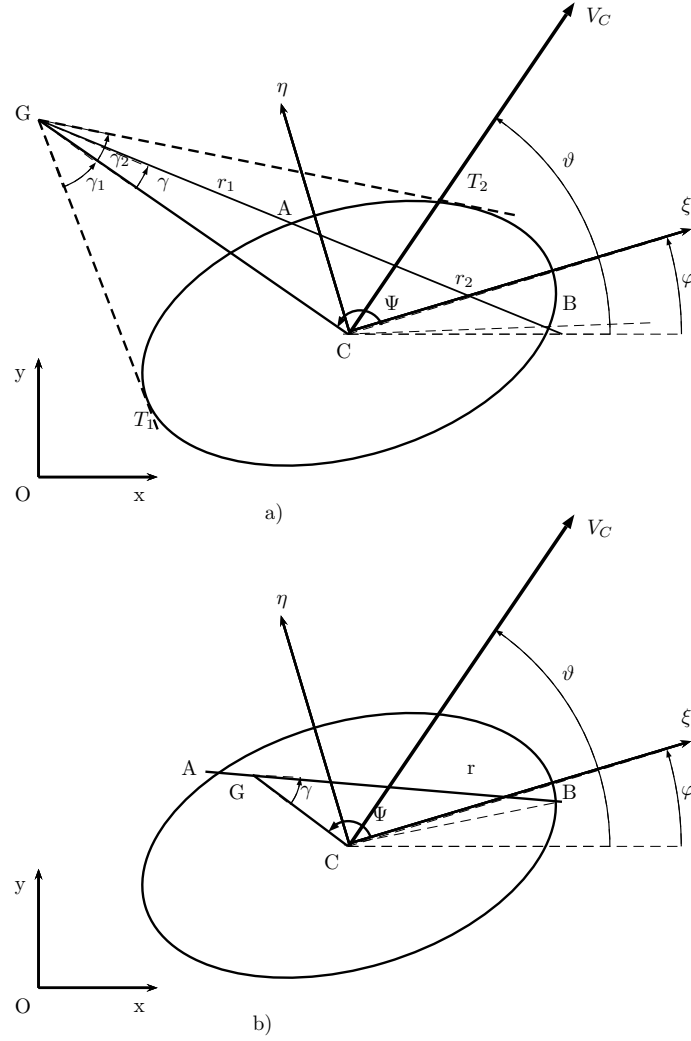


Figure 1: Coordinate system. Method A.I. Lurye: instantaneous velocity center, a) outside area, b) inside area

Let's find integration ranges in (8). We introduce angle $\Psi = \frac{\pi}{2} + \vartheta - \varphi$ (see fig. 1). If the point G is inside elliptical plate, distance r from G to the border of contacting area B can be found from:

$$\frac{(GB \cos(\pi - (\Psi + \gamma)) - \xi_G)^2}{a^2} + \frac{(GB \sin(\pi - (\Psi + \gamma)) - \eta_G)^2}{b^2} = 1,$$

here coordinates of instantaneous velocity center are:

$$\xi_G = x_G \cos \varphi + y_G \sin \varphi, \quad \eta_G = -x_G \sin \varphi + y_G \cos \varphi,$$

$$x_G = -\frac{v}{\omega} \sin \vartheta, \quad y_G = \frac{v}{\omega} \cos \vartheta.$$

Thus, we receive:

$$r = GB = \frac{\lambda_1 + abD_1}{\lambda_2}, \quad (9)$$

where

$$\begin{aligned} \lambda_1 &= b^2 \xi_G \cos(\Psi + \gamma) + a^2 \eta_G \sin(\Psi + \gamma), \\ \lambda_2 &= b^2 \cos^2(\Psi + \gamma) + a^2 \sin^2(\Psi + \gamma), \end{aligned}$$

$$D_1 = \sqrt{(b^2 - \eta_G^2) \cos^2(\Psi + \gamma) + (a^2 - \xi_G^2) \sin^2(\Psi + \gamma) + \xi_G \eta_G \sin(2(\Psi + \gamma))}.$$

Angle γ in equation (9) takes values from 0 to 2π (see [19]).

The same calculations for the point G outside the area lead to the following:

$$\begin{aligned} r_1 = GA &= \frac{\lambda_1 - abD_1}{\lambda_2}, \\ r_2 = GB &= \frac{\lambda_1 + abD_1}{\lambda_2}. \end{aligned} \quad (10)$$

Let's find angles γ_1 and γ_2 for that case. Points where line GA intersects ellipse in coordinate system $C\xi\eta$ can be found from the system of equations:

$$\begin{aligned} \frac{\xi_A^2}{a^2} + \frac{\eta_A^2}{b^2} &= 1, \\ \eta_A &= \xi_A k + \sigma, \end{aligned}$$

where

$$\sigma = \eta_G - \xi_G k, \quad k = \tan\left(\frac{\pi}{2} + \vartheta - \varphi + \gamma\right).$$

The line will be tangent to ellipse if the following equation is satisfied:

$$\sigma^2 = a^2 k^2 + b^2.$$

We receive equation for parameter k :

$$(\xi_G^2 - a^2)k^2 - 2\eta_G \xi_G k + \eta_G^2 - b^2 = 0.$$

Thus:

$$k_{1,2} = \frac{\eta_G \xi_G \pm \sqrt{\xi_G^2 b^2 + a^2 \eta_G^2 - a^2 b^2}}{\xi_G^2 - a^2},$$

and, finally,

$$\gamma_{1,2} = \arctan(k_{1,2}) - \frac{\pi}{2} - \vartheta + \varphi. \quad (11)$$

We can rewrite forces in dimensionless form taking into account the following relations:

$$I = \rho \pi \kappa a^4 I^*, \quad \xi = a \xi^*, \quad \eta = a \kappa \eta^*, \quad \beta = \beta^* a, \quad p = p^* \frac{mg}{\pi ab},$$

here asterisks are dedicated to dimensionless variables: I^* is a dimensionless inertia moment, ξ^*, η^* are dimensionless coordinates (asterisks for these variables are omitted later).

Thus, we can write components of total friction force and total moment in the case, when instantaneous velocity center lies inside the contact area:

$$\begin{aligned} T_x^* &= -f_x \int_0^{2\pi} \cos(\vartheta + \gamma) \left(\frac{\kappa(\lambda_1^* + D_1^*)^2}{2\lambda_2^{*2}} \right) d\gamma, \\ T_y^* &= -f_y \int_0^{2\pi} \sin(\vartheta + \gamma) \left(\frac{\kappa(\lambda_1^* + D_1^*)^2}{2\lambda_2^{*2}} \right) d\gamma, \\ M_G^* &= - \int_0^{2\pi} \left(f_x + \frac{\mu}{2} - \frac{\mu}{2} \cos(2\vartheta + 2\gamma) \right) \left(\frac{\kappa^2(\lambda_1^* + D_1^*)^3}{3\lambda_2^{*3}} \right) d\gamma, \\ M_C^* &= M_G^* - \int_0^{2\pi} \beta \left(\frac{\mu}{2} \cos(\gamma) - \frac{\mu}{2} \cos(2\vartheta + \gamma) + f_x \cos(\gamma) \right) \left(\frac{\kappa(\lambda_1^* + D_1^*)^2}{2\lambda_2^{*2}} \right) d\gamma. \end{aligned} \quad (12)$$

And in the case, when instantaneous velocity center is outside the contact area:

$$\begin{aligned} T_x^* &= -f_x \int_{\gamma_1}^{\gamma_2} \cos(\vartheta + \gamma) \left(\frac{2\kappa D_1^* \lambda_1^*}{\lambda_2^{*2}} \right) d\gamma, \\ T_y^* &= -f_y \int_{\gamma_1}^{\gamma_2} \sin(\vartheta + \gamma) \left(\frac{2\kappa D_1^* \lambda_1^*}{\lambda_2^{*2}} \right) d\gamma, \\ M_G^* &= - \int_{\gamma_1}^{\gamma_2} \left(f_x + \frac{\mu}{2} - \frac{\mu}{2} \cos(2\vartheta + 2\gamma) \right) \left(\frac{\kappa^2 (2D_1^{*3} + 6D_1^* \lambda_1^{*2})}{3\lambda_2^{*3}} \right) d\gamma, \\ M_C^* &= M_G^* - \int_{\gamma_1}^{\gamma_2} \beta \left(\frac{\mu}{2} \cos(\gamma) - \frac{\mu}{2} \cos(2\vartheta + \gamma) + f_x \cos(\gamma) \right) \left(\frac{2\kappa D_1^* \lambda_1^*}{\lambda_2^{*2}} \right) d\gamma, \end{aligned} \quad (13)$$

where

$$\lambda_1^* = \kappa \xi_G \cos(\Psi + \gamma) + \eta_G \sin(\Psi + \gamma),$$

$$\lambda_2^* = \kappa^2 \cos^2(\Psi + \gamma) + \sin^2(\Psi + \gamma),$$

$$D_1^* = \sqrt{\kappa^2(1 - \eta_G^2) \cos^2(\Psi + \gamma) + (1 - \xi_G^2) \sin^2(\Psi + \gamma) + \kappa \xi_G \eta_G \sin(2(\Psi + \gamma))}.$$

3.2 Asymmetric orthotropic friction

Equations (12) and (13) achieved in the previous section for symmetric orthotropic friction are suitable for asymmetric case as well. However, we should evaluate another integration ranges. In this case it is important to know directions of sliding velocities. Each area on figure 2 corresponds to different cases of velocities orientation and, thus, different friction coefficients.

We have to find rules for positioning instantaneous velocity center G in each area. Let's introduce points $p1, p2, p3, p4$, which are coordinates of tangents to ellipse parallel to axes Cx and Cy .

In system $C\xi\eta$: equation of line p_3 is $\eta = k_3\xi + l_3$, with $k_3 = -\tan\varphi$. Coordinates of contact point in system $C\xi\eta$ can be found from the following relations:

$$\eta = -\tan\varphi\xi + l_3,$$

$$\frac{\xi^2}{a^2} + \frac{\eta^2}{b^2} = 1.$$

Taking $l_3 = \sqrt{a^2k_3^2 + b^2}$ we obtain

$$\xi_{p3} = -\frac{a^2k_3}{\sqrt{a^2k_3^2 + b^2}},$$

$$\eta_{p3} = k_3\xi_{p3} + l_3,$$

and in system Cxy we get:

$$x_{p3} = \xi_{p3} \cos\varphi - \eta_{p3} \sin\varphi,$$

$$y_{p3} = \xi_{p3} \sin\varphi + \eta_{p3} \cos\varphi.$$

The same idea is useful for other 3 points with: $k_1 = \cot\varphi$, $l_1 = \sqrt{a^2k_1^2 + b^2}$, $k_2 = \cot\varphi$, $l_2 = -l_1$, $k_4 = -\tan\varphi$, $l_4 = -l_3$.

Now take a look at area 7 (see table 2). It is divided into 4 parts. Each part contains points with velocities directed to the same quadrant. That means that for each of the part coefficients of friction remain constant. So projections of the

friction force and the moment are:

$$\begin{aligned}
T_x^* &= - \sum_{i=0, j=1}^{i=4, j=5} \int_{\psi_i}^{\psi_j} f_x^{ij} \cos(\vartheta + \gamma) \left(\frac{\kappa(\lambda_1^* + D_1^*)^2}{2\lambda_2^{*2}} \right) d\gamma, \\
T_y^* &= - \sum_{i=0, j=1}^{i=4, j=5} \int_{\psi_i}^{\psi_j} f_y^{ij} \sin(\vartheta + \gamma) \left(\frac{\kappa(\lambda_1^* + D_1^*)^2}{2\lambda_2^{*2}} \right) d\gamma, \\
M_G^* &= - \sum_{i=0, j=1}^{i=4, j=5} \int_{\psi_i}^{\psi_j} \left(f_x^{ij} + \frac{\mu^{ij}}{2} - \frac{\mu^{ij}}{2} \cos(2\vartheta + 2\gamma) \right) \left(\frac{\kappa^2(\lambda_1^* + D_1^*)^3}{3\lambda_2^{*3}} \right) d\gamma, \\
M_C^* &= M_G^* - \sum_{i=0, j=1}^{i=4, j=5} \int_{\psi_i}^{\psi_j} \beta \left(\frac{\mu^{ij}}{2} \cos(\gamma) - \frac{\mu^{ij}}{2} \cos(2\vartheta + \gamma) + f_x^{ij} \cos(\gamma) \right) \left(\frac{\kappa(\lambda_1^* + D_1^*)^2}{2\lambda_2^{*2}} \right) d\gamma.
\end{aligned} \tag{14}$$

In (14) the area integral from (12) is partitioned to 5 integrals with constant values of friction coefficients with $\psi_0 = 0$, $\psi_1 = \alpha_1$, $\psi_2 = \alpha_2$, $\psi_3 = \alpha_3$, $\psi_4 = \alpha_4$, $\psi_5 = \alpha_5$ and $\sum \psi_i = 2\pi$ (see table 2).

Tables 1 and 2 show the way how equations (13) are divided into several parts. Thus, finally, we achieve equations for friction force projections in the case of instantaneous velocity center lies outside area covered by the plate in the following form:

$$\begin{aligned}
T_x^* &= - \sum_{i=0, j=1}^{i=z-1, j=z} \int_{\psi_i}^{\psi_j} f_x^{ij} \cos(\vartheta + \gamma) \left(\frac{2\kappa D_1^* \lambda_1^*}{\lambda_2^{*2}} \right) d\gamma, \\
T_y^* &= - \sum_{i=0, j=1}^{i=z-1, j=z} \int_{\psi_i}^{\psi_j} f_y^{ij} \sin(\vartheta + \gamma) \left(\frac{2\kappa D_1^* \lambda_1^*}{\lambda_2^{*2}} \right) d\gamma, \\
M_G^* &= - \sum_{i=0, j=1}^{i=z-1, j=z} \int_{\psi_i}^{\psi_j} \left(f_x^{ij} + \frac{\mu^{ij}}{2} - \frac{\mu^{ij}}{2} \cos(2\vartheta + 2\gamma) \right) \left(\frac{\kappa^2 (2D_1^{*3} + 6D_1^* \lambda_1^{*2})}{3\lambda_2^{*3}} \right) d\gamma, \\
M_C^* &= M_G^* - \sum_{i=0, j=1}^{i=z-1, j=z} \int_{\psi_i}^{\psi_j} \beta \left(\frac{\mu^{i,j}}{2} \cos(\gamma) - \frac{\mu^{ij}}{2} \cos(2\vartheta + \gamma) + f_x \cos(\gamma) \right) \left(\frac{2\kappa D_1^* \lambda_1^*}{\lambda_2^{*2}} \right) d\gamma.
\end{aligned} \tag{15}$$

Table 1: Velocities distribution and integration ranges evaluation. Part 1.

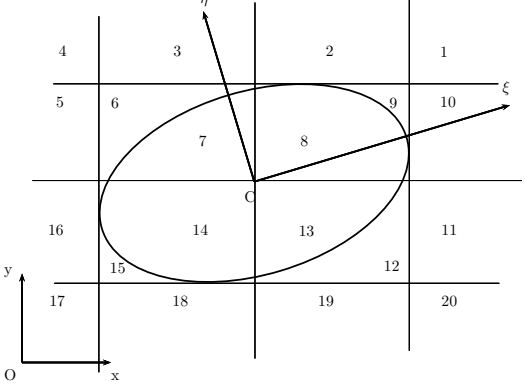
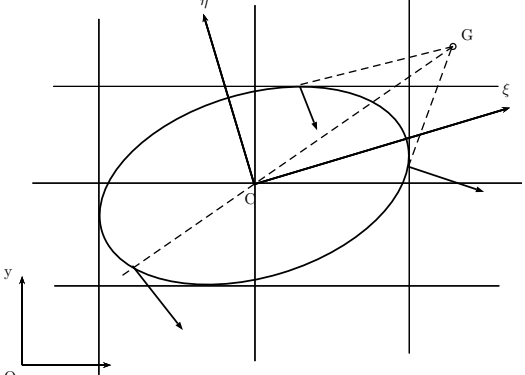
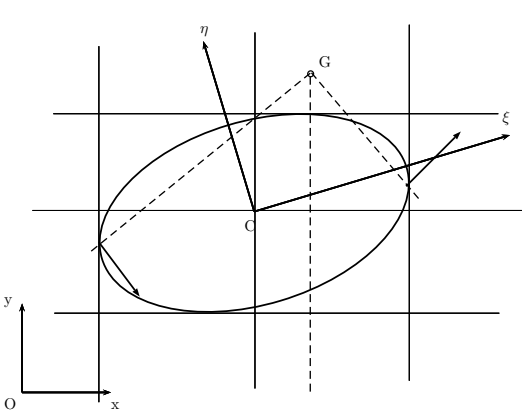
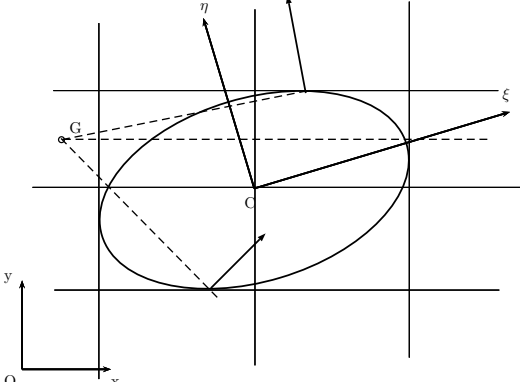
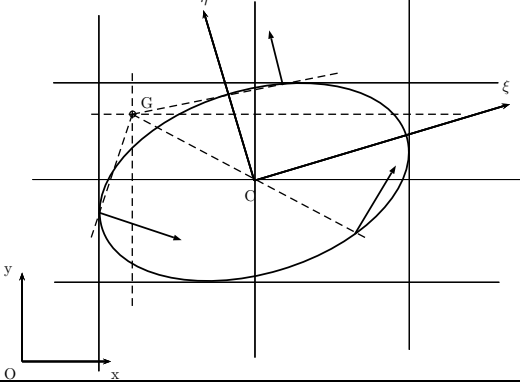
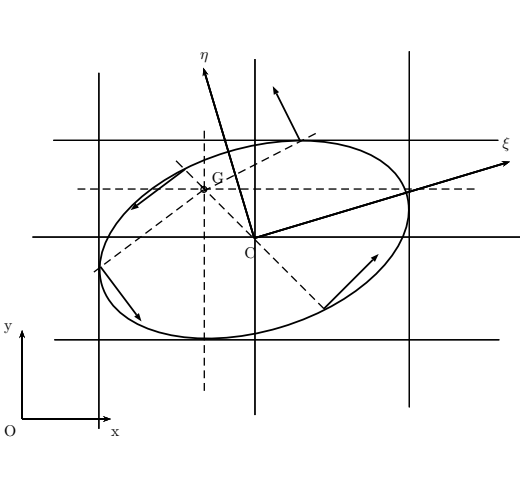
 <p>Figure 2: Splitting geometry</p>	<p>Here each partition correspond to different velocity directions distribution.</p>
	<p>Area 1, velocities oriented to the III quadrant. $x_G > x_{p1}, \quad y_G > y_{p3}$ $z = 1, \psi_0 = -\gamma_1, \psi_1 = \gamma_2$ $f_x^{01} = f_{x+}, f_y^{01} = f_{y-}$ For areas 1, 4, 17, 20 all velocities are directed to the same quadrant.</p>
	<p>Area 2, velocities oriented to the I and IV quadrants. $x_G > 0, \quad x_G \leq x_{p1},$ $y_G > y_{p3},$ $\alpha = \arctan \frac{x_G}{y_G}$ $z = 2, \psi_0 = -\gamma_1, \psi_1 = \alpha, \psi_2 = \gamma_2$ $f_x^{01} = f_{x+}, f_y^{01} = f_{y-},$ $f_x^{12} = f_{x+}, f_y^{12} = f_{y+}$ For areas 2, 3, 18, 19 all velocities are directed to 2 quadrants and the line separating the parts is parallel to axis Oy.</p>

Table 2: Sliding velocities distributions and integration ranges evaluations. Part 2.

	<p>Area 5, velocities oriented to the I and II quadrants.</p> $x_G \leq x_{p2}, y_G > 0, \quad y_G \leq y_{p3}, \alpha = \arctan \frac{y_G}{x_G}$ $z = 2, \psi_0 = -\gamma_1, \psi_1 = \alpha, \psi_2 = \gamma_2$ $f_x^{01} = f_{x+}, f_y^{01} = f_{y+}$ $f_x^{12} = f_{x-}, f_y^{12} = f_{y+}$ <p>For areas 5, 10, 11, 16 all velocities are directed to 2 quadrants and the line separating the parts is parallel to axis Ox.</p>
	<p>Area 6, velocities oriented to the I, II and IV quadrants.</p> $x_G \leq 0, \quad x_G > x_{p2}, y_G > y_{p2}, \quad y_G \leq y_{p3},$ $\frac{\xi_G^2}{a^2} + \frac{\eta_G^2}{b^2} > 1, \alpha_1 = \arctan \frac{x_G}{y_G}, \alpha_2 = \arctan \frac{y_G}{x_G}$ $f_x^{01} = f_{x+}, f_y^{01} = f_{y+}$ $f_x^{12} = f_{x-}, f_y^{12} = f_{y+}$ $f_x^{23} = f_{x+}, f_y^{23} = f_{y-}$ <p>For areas 6, 9, 12, 15 all velocities are directed to 3 quadrants.</p>
	<p>Area 7, velocities are directed to I, II, III, IV quadrants.</p> $\alpha_1 = \arctan \frac{y_G}{x_G}, \alpha_2 = \alpha_1 + \frac{\pi}{2}, \alpha_3 = \alpha_2 + \frac{\pi}{2},$ $\alpha_4 = \alpha_3 + \frac{\pi}{2}, \alpha_5 = \alpha_4 + \arctan \frac{x_G}{y_G},$ $x_G \leq 0, y_G > 0, \frac{\xi_G^2}{a^2} + \frac{\eta_G^2}{b^2} \leq 1,$ $f_x^{01} = f_{x+}, f_y^{01} = f_{y+}$ $f_x^{12} = f_{x-}, f_y^{12} = f_{y+}$ $f_x^{23} = f_{x-}, f_y^{23} = f_{y-}$ $f_x^{34} = f_{x+}, f_y^{34} = f_{y-}$ <p>For areas 6, 8, 13, 14 velocities are directed to all 4 quadrants.</p>

4 Selected results

4.1 General considerations

Let's divide the first equation of the system (6) by the third and let's introduce derived right part $\Phi_1(\beta, \vartheta)$:

$$\begin{aligned} \frac{dv_C}{d\omega} &= \Phi_1(\beta, \vartheta), \\ v_C \frac{d\vartheta}{dt} &= T_n(\beta, \vartheta). \end{aligned} \tag{16}$$

The dissipative friction force has negative power, thus, motion with non-zero initial conditions terminates (the plate moves a finite period of time). Thus, second equation in the system (16) allows us to write a relation:

$$T_n(\beta, \vartheta) \xrightarrow[t \rightarrow t_*]{\vartheta \rightarrow \vartheta_* \atop \beta \rightarrow \beta_*} 0, \quad (17)$$

where ϑ_* and β_* are limit values of corresponding parameters, t_* is a terminal moment. Integrating first equation of the system (16) we achieve:

$$\omega = \omega_0 \exp \left[- \int_{\beta_0}^{\beta_1} \frac{d\beta}{\beta - \Phi_1(\beta, \vartheta)} \right]. \quad (18)$$

It is important to mention, that function $\Phi_1(\beta, \vartheta)$ depends not only on β and ϑ but also on the shape of the contact area, pressure distribution law $p(\xi, \eta)$, components of the friction matrix f_x , f_y and the angle φ (orientation of the body on the surface). Thus, value of β_1 , when integral in (18) becomes improper and seeks $-\infty$, depends on parameters of the mechanical system:

$$\beta_1 \xrightarrow[t \rightarrow t_*]{\vartheta \rightarrow \vartheta_* \atop \varphi \rightarrow \varphi_*} \beta_*(\vartheta_*, \varphi_*, \Omega, f_x, f_y, p(\xi, \eta)). \quad (19)$$

Summarizing, note that by the time t_* relation (17) and

$$\beta - \Phi_1(\beta, \vartheta) \xrightarrow[t \rightarrow t_*]{\vartheta \rightarrow \vartheta_* \atop \beta \rightarrow \beta_*} 0. \quad (20)$$

should be achieved.

Furthermore, with fixed values of $\beta = \tilde{\beta}$ equations $T_n(\tilde{\beta}, \vartheta) = 0$ and (20) may have several solutions. However, both conditions (17) and (20) are achieved with singular ϑ_* , β_* [7], which depend on initial conditions.

It is important to mention that from system (6) with introducing parameter $\delta = \beta^{-1}$ we may derive the following system of equations:

$$\begin{aligned} \frac{d\omega}{dv_C} &= \Phi_2(\delta, \vartheta), \\ v_C \frac{d\vartheta}{dt} &= T_n(\delta, \vartheta). \end{aligned} \quad (21)$$

From system (21) we achieve:

$$T_n(\delta, \vartheta) \xrightarrow[t \rightarrow t_*]{\vartheta \rightarrow \vartheta_* \atop \delta \rightarrow \delta_*} 0, \quad (22)$$

and

$$v_C = v_{C0} \exp \left[- \int_{\delta_0}^{\delta_1} \frac{d\delta}{\Phi_2(\delta, \vartheta) - \delta} \right], \quad (23)$$

and, finally, with same reasoning:

$$\Phi_2(\delta, \vartheta) - \delta \xrightarrow[\substack{t \rightarrow t_* \\ \vartheta \rightarrow \vartheta_* \\ \delta \rightarrow \delta_*}]{0} 0. \quad (24)$$

During searching limit values of ϑ_* , δ_* with equations (17) and (20), it may occur that there are no roots. Thus, we should solve equations (22) and (24) to find ϑ_* , δ_* . Furthermore, because there is a strict dependence of plate motion on interrelations between inertia moment and friction coefficients (see, for example, [8]) we should all the time check solution in both regions.

4.2 Symmetric orthotropic friction. Specific initial conditions of motion

4.2.1 Initial conditions of motion $\omega = 0$, $v \neq 0$

Let's get back to system (5). With (3) and (4) it is possible to show that in case $\omega = 0$, $v \neq 0$ we have:

$$\begin{aligned} \tau_x &= -p(f_x \cos \vartheta + f \sin \vartheta), \\ \tau_y &= -p(-f \cos \vartheta + f_y \sin \vartheta), \end{aligned}$$

and, thus, we achieve system:

$$\begin{aligned} m\dot{v}_C &= T_x \cos \vartheta + T_y \sin \vartheta = -p \iint_{\Omega} (\mu \sin^2 \vartheta + f_x) d\xi d\eta, \\ m v_C \dot{\vartheta} &= -T_x \sin \vartheta + T_y \cos \vartheta = -p \iint_{\Omega} (\mu \sin \vartheta \cos \vartheta - f) d\xi d\eta, \\ I\dot{\omega} &= \iint_{\Omega} (\tau_y x' - \tau_x y') d\xi d\eta = -p \iint_{\Omega} (\xi K_1 + \eta K_2) d\xi d\eta, \end{aligned} \quad (25)$$

where

$$\begin{aligned} K_1 &= (\mu \sin \vartheta \cos \varphi + f_x \sin(\vartheta - \varphi) - f \cos(\vartheta - \varphi)), \\ K_2 &= (-\mu \sin \vartheta \sin \varphi - f_x \cos(\vartheta - \varphi) - f \cos(\vartheta - \varphi)). \end{aligned}$$

It can be shown that integrals in the third equation of system (25) is equal to zero for elliptical and circular contact areas. So, finally we have:

$$\begin{aligned} m\dot{v}_C &= -pS(\mu \sin^2 \vartheta + f_x), \\ m\dot{v}_C \dot{\vartheta} &= -pS(\mu \sin \vartheta \cos \vartheta - f), \\ I\dot{\omega} &= 0. \end{aligned} \quad (26)$$

From the system of equations (26) we see, that in case the initial motion is translational it stays translational until the final point.

4.2.2 Initial conditions of motion $\omega \neq 0$, $v = 0$

For equation (5) taking into account conditions $v = 0$, $\omega \neq 0$ we have that parameter β is zero and from (3) and (4) we achieve system of equations:

$$\begin{aligned} m\dot{v}_C &= -p \iint_{\Omega} \frac{\xi A_0 + \eta A_1}{D} d\xi d\eta = -p[A_0 F_1(\xi, \eta) + A_1 G_1(\xi, \eta)], \\ m\dot{v}_C \dot{\vartheta} &= -p \iint_{\Omega} \frac{\xi B_0 + \eta B_1}{D} d\xi d\eta = -p[B_0 F_1(\xi, \eta) + B_1 G_1(\xi, \eta)], \\ I\dot{\omega} &= -p \iint_{\Omega} \frac{\xi^2 C_0 + \xi \eta C_1 + \eta^2 C_2}{D} d\xi d\eta = -p[C_0 F_2(\xi, \eta) + C_1 L(\xi, \eta) + C_2 G_2(\xi, \eta)], \end{aligned} \quad (27)$$

where

$$\begin{aligned} D &= \sqrt{\xi^2 + \eta^2}, \\ A_0 &= \mu \cos \varphi \sin \vartheta + f_x \sin(\vartheta - \varphi) + f \cos(\vartheta - \varphi), \\ A_1 &= f \sin(\vartheta - \varphi) - \mu \sin \vartheta \sin \varphi - f_x \cos(\vartheta - \varphi), \\ B_0 &= \mu \cos \varphi \cos \vartheta + f_x \cos(\vartheta - \varphi) - f \sin(\vartheta - \varphi), \\ B_1 &= f \cos(\vartheta - \varphi) + f_x \sin(\vartheta - \varphi) - \mu \sin \varphi \cos \vartheta, \\ C_0 &= f_x + \mu \cos^2 \varphi, \quad C_1 = -2\mu \cos \varphi \sin \varphi, \quad C_2 = f_x + \mu \sin^2 \varphi. \\ F_1(\xi, \eta) &= \iint_{\Omega} \frac{\xi}{\sqrt{\xi^2 + \eta^2}} d\xi d\eta, \quad G_1(\xi, \eta) = \iint_{\Omega} \frac{\eta}{\sqrt{\xi^2 + \eta^2}} d\xi d\eta, \\ F_2(\xi, \eta) &= \iint_{\Omega} \frac{\xi^2}{\sqrt{\xi^2 + \eta^2}} d\xi d\eta, \quad G_2(\xi, \eta) = \iint_{\Omega} \frac{\eta^2}{\sqrt{\xi^2 + \eta^2}} d\xi d\eta, \\ L(\xi, \eta) &= \iint_{\Omega} \frac{\xi \eta}{\sqrt{\xi^2 + \eta^2}} d\xi d\eta. \end{aligned}$$

Now we find integrals $F_1(\xi, \eta)$, $G_1(\xi, \eta)$, $F_2(\xi, \eta)$, $G_2(\xi, \eta)$, $L(\xi, \eta)$. It can be seen that for $F_1(\xi, \eta)$, $G_1(\xi, \eta)$ and $L(\xi, \eta)$ the integration area is symmetrical, thus:

$$\begin{aligned} F_1(\xi, \eta) &= \int_{-b}^b d\eta \int_{-ah_2(\eta)}^{ah_2(\eta)} \frac{\xi}{\sqrt{\xi^2 + \eta^2}} d\xi = 0, & G_1(\xi, \eta) &= \int_{-a}^a d\xi \int_{-bh_1(\xi)}^{bh_1(\xi)} \frac{\eta}{\sqrt{\xi^2 + \eta^2}} d\eta = 0, \\ L(\xi, \eta) &= \int_{-b}^b \eta d\eta \int_{-ah_2(\eta)}^{ah_2(\eta)} \frac{\xi}{\sqrt{\xi^2 + \eta^2}} d\xi = 0, & h_1 &= \sqrt{1 - \frac{\xi^2}{a^2}}, & h_2 &= \sqrt{1 - \frac{\eta^2}{b^2}}. \end{aligned} \quad (28)$$

Integrals $F_2(\xi, \eta)$, $G_2(\xi, \eta)$ are not equal to zero for the area.

$$\begin{aligned} F_2(\xi, \eta) &= \int_{-b}^b d\eta \int_{-ah_2(\eta)}^{ah_2(\eta)} \frac{\xi^2}{\sqrt{\xi^2 + \eta^2}} d\xi = - \int_{-b}^b \frac{\eta^2}{2} \ln \frac{\left(\sqrt{a^2 h_2^2(\eta) + \eta^2} + ah_2(\eta)\right)^2}{\eta^2} d\eta, \\ G_2(\xi, \eta) &= \int_{-a}^a d\xi \int_{-bh_1(\xi)}^{bh_1(\xi)} \frac{\eta^2}{\sqrt{\xi^2 + \eta^2}} d\eta = - \int_{-a}^a \frac{\xi^2}{2} \ln \frac{\left(\sqrt{b^2 h_1^2(\xi) + \xi^2} + bh_1(\xi)\right)^2}{\xi^2} d\xi. \end{aligned} \quad (29)$$

Thus equations(27) transform into:

$$\begin{aligned} m\dot{v}_C &= 0, \\ m v_C \dot{\vartheta} &= 0, \\ I\dot{\omega} &= C_0 F_2(\xi, \eta) + C_2 G_2(\xi, \eta). \end{aligned} \quad (30)$$

For symmetric orthotropic friction and uniform pressure distribution it can be stated that if the initial motion is rotational it stays rotational until the end.

4.3 Symmetric and asymmetric orthotropic friction. Numerical results

If the initial values of angular and linear (sliding) velocities are non-zero any analytic simplifications can hardly be reached. In our paper [11] system of equations (6) was solved in (ξ, η) coordinate system, but with this approach an accuracy of results was not enough satisfied. Furthermore, at the most final points the method tends to give significant oscillations, because near $\beta = \beta_*$ situation with singularity may appear. So we switched to the method Lurye described here. After

manipulations with forces integrals according to the described method, we obtained a very stable and accurate numerical procedure. With this new approach we achieved numerical solution for uniform pressure distribution and symmetric and asymmetric friction forces.

Table 3 shows resultant values of parameters of interest for circular and elliptic plates. The instantaneous velocity center for both types of plates is located in the same area. However, velocity vector rotational angle ϑ_* is noticeably higher for elliptic plate. Instantaneous velocity center position described by β_* is lower for elliptic plate comparing with circular one.

In our paper [12] results for symmetric orthotropic case were presented. For symmetric case β_* is significantly lower for both circular and elliptic plates comparing to asymmetric example. Furthermore, for circular plate in symmetric orthotropic friction we have $\vartheta_* = 0$. However, in asymmetric case for both shapes ϑ_* values show that velocity vector orients to the 3rd quadrant, which is actually the one with the lowest coefficients of friction.

Table 3: Parameters β_* , ϑ_* for circular and elliptical plates for asymmetric orthotropic friction ($\vartheta_0 = \frac{\pi}{4}$, $\varphi_0 = \frac{\pi}{3}$)

	Circle			Ellipse ($e = 0.6$)		
μ_+	β_*	ϑ_*	Area	β_*	ϑ_*	Area
0.03	0.887	-2.46	13	0.81	-2.71	13
0.06	0.908	-2.57	13	0.83	-2.77	13
0.09	0.937	-2.65	13	0.86	-2.82	13
0.12	0.976	-2.71	13	0.89	-2.86	13
0.15	1.042	-2.78	12	0.91	-2.88	12
0.18	1.197	-2.86	19	0.99	-2.93	19

Figure 3 demonstrates evolution of $\beta(t)$, $\vartheta(t)$ for symmetric and asymmetric cases. It was assumed that $a = 1$ and represents major semi-axes of elliptic plate, which eccentricity is $e = 0.6$ and for circular plate $e = 0$. Initial conditions taken in the example are: $v_0 = 1$, $\omega_0 = 1$, $\vartheta_0 = \pi/4$, and initial ellipse orientation angle is $\varphi_0 = \pi/3$. Friction coefficient $\mu_+ = f_{y+} - f_{x+}$ with $f_x = f_{x+} = 0.42$, $f_{x-} = 0.5f_{x+}$, $f_y = f_{y+}$, $f_{y-} = 0.5f_{y+}$. For both symmetric and asymmetric cases sliding and spinning end simultaneously. This important outcome was also achieved for non-uniform pressure distributions: for circular plate with respect to isotropic friction force and axisymmetric normal pressure in [2], under linear pressure distribution in [4], and for elliptic plate under linear pressure distribution and symmetric orthotropic friction in [11]. However, figure

shows significant difference in behavior of $\beta(t)$, $\vartheta(t)$ curves with respect to asymmetry of friction force. Shape factor is noticeably important for both symmetric and asymmetric cases: elliptic plate moves shorter period of time with more velocity vector rotation (higher changes of ϑ values).

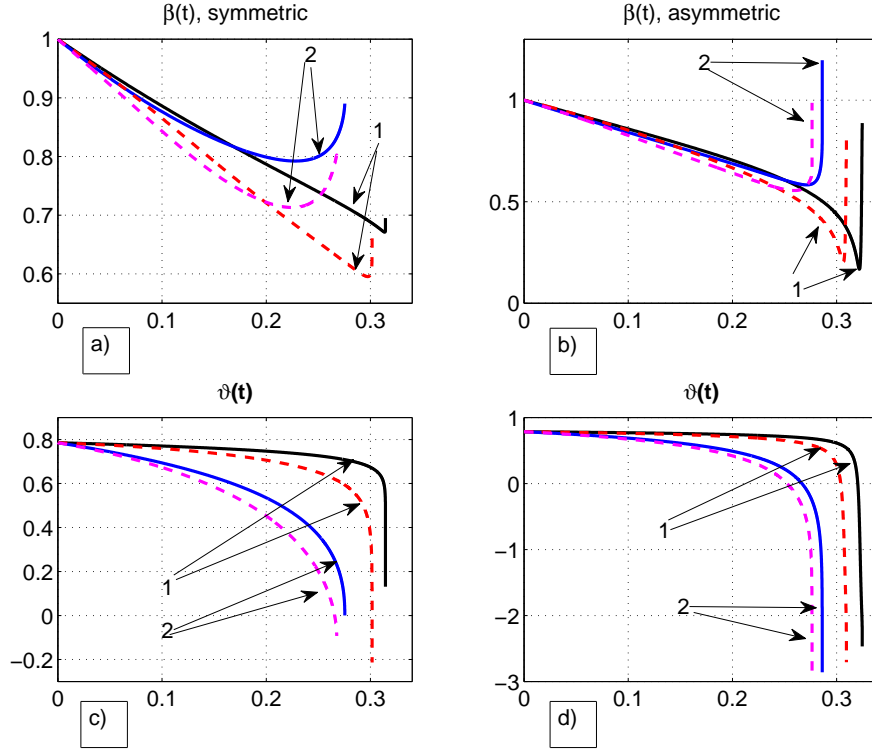


Figure 3: Parameters β and ϑ evolution for circular (solid line) and elliptic (dashed line) plate for orthotropic friction: (1) $\mu = \mu_+ = 0.03$, (2) $\mu = \mu_+ = 0.18$

5 Conclusion

- Problem of terminal motion of thin elliptic plate taking into account anisotropy of friction force is formulated. General analytic results show that it is possible to analyze the system of motion equations without specifying pressure distribution. It is stated that until the terminal point two conditions (20) and (17) should be achieved simultaneously.
- Total friction force and total moment evaluations are shown in the case of thin elliptic plate under uniform pressure distribution. Two cases are discussed: symmetric orthotropic friction and asymmetric orthotropic friction.

Based on the Lurye method friction force is obtained for both cases. This leads to significant simplifications of numerical procedure.

- Some specific cases of initial conditions are analyzed separately with the aid of numerical study. It is shown, that for symmetric orthotropic friction and elliptic contact area under uniform pressure distribution: if the initial motion is linear it stays linear till the end. In case initial motion is rotational it is rotational during the whole period of motion.
- Numerical results are presented for symmetric and asymmetric friction forces and elliptic and circular contact areas under uniform pressure distribution. It is stated that sliding and spinning end simultaneously both in symmetric and asymmetric cases. Figures show significant influence of asymmetry of friction forces on the motion. Contact area impact is also pointed out.

References

- [1] ANTONI, N., LIGIER, J.-L., SAFFRE, P., AND PASTOR, J. Asymmetric friction: Modeling and experiments. *Int.J.Eng. Sci.* 45 (2007), 587–600.
- [2] ARGATOV, I. Equilibrium conditions for a rigid body on a rough plane in the case of axially symmetric distribution of normal pressures. *Mech. Solids* 40, 2 (2005), 11–20.
- [3] BAFEKRPOUR, E., DYSKIN, A., PASTERNAK, E., MOLOTNIKOV, A., AND ESTRIN, Y. Internally architected materials with directionally asymmetric friction. *Scientific Reports* 5 (2015), 10732 EP.
- [4] BORISOV, A., KARAVAEV, Y., MAMAEV, I., ERDAKOVA, N., IVANOVA, T., AND TARASOV, V. Experimental investigation of the motion of a body with an axisymmetric base sliding on a rough plane. *Regular and Chaotic Dynamics* 20, 5 (2015), 518–541.
- [5] CAMPIONE, M., TRABATTONI, S., AND MORET, M. Nanoscale mapping of frictional anisotropy. *Tribol Lett* 45, 219–224 (2012).
- [6] CARBONE, G., MALCHIKOV, A., CECCARELLI, M., AND JATSUN, S. Design and simulation of kursk robot for in-pipe inspection. In *Proceedings of the 10th IFToMM International Symposium on Science of Mechanisms and Machines* (Brasov, Romania, October 12–15 2009), Springer, pp. 103–114.
- [7] DMITRIEV, N. Movement of the disk and the ring over the plane with anisotropic friction. *J.Fric. Wear* 23 (2002), 10–15.

- [8] DMITRIEV, N. Sliding of a solid body supported by a round platform on a horizontal plane with orthotropic friction. part 1. regular load distribution. *J.Fric. Wear* 30, 4 (2009), 227–234.
- [9] DMITRIEV, N. Motion of material point and equilibrium of two-mass system under asymmetric orthotropic friction. *J.Fric. Wear* 34 (2013), 429–437.
- [10] DMITRIEV, N. Motion of a narrow ring on a plane with asymmetric orthotropic friction. *J.Fric. Wear* 36 (2015), 80–88.
- [11] DMITRIEV, N., AND SILANTYEVA, O. About the movement of a solid body on a plane surface in accordance with elliptic contact area and anisotropic friction force. In *Proc. of jointly organised WCCM XI, ECCM V, ECFD VI. Vol. IV* (Barcelona, Spain, 2014), vol. 4, CIMNE, pp. 4440–4452.
- [12] DMITRIEV, N., AND SILANTYEVA, O. Terminal motion of a thin elliptical plate over a horizontal plane with orthotropic friction. *Vestnik St. Petersburg University: Mathematics* 49, 1 (2016), 92–98.
- [13] FARKAS, Z., BARTELS, G., UNGER, T., AND WOLF, D. Frictional coupling between sliding and spinning motion. *Phys. Rev. Lett.* 90, 24 (2003), 248–302.
- [14] ISHIGAMI, G., OVERHOLT, J., AND IAGNEMMA, K. Multi-material anisotropic friction wheels for omnidirectional ground vehicles. *Journal of Robotics and Mechatronics* 24 (2012), 261–267.
- [15] KONYUKHOV, A., VIELSACK, P., AND SCHWEIZERHOF, K. On coupled models of anisotropic contact surfaces and their experimental validation. *Wear* 264 (2008), 579–588.
- [16] LOPES, D. S., NEPTUNE, R. R., AMBRÓSIO, J. A., AND SILVA, M. T. A superellipsoid-plane model for simulating foot-ground contact during human gait. *Computer Methods in Biomechanics and Biomedical Engineering* (2015), 1–10.
- [17] LURYE, A. *Analytical Mechanics*. Springer-Verlag Berlin Heidelberg, Berlin, 2002.
- [18] PIOTROWSKI, J., AND CHOLLET, H. Wheel-rail contact models for vehicle system dynamics including multi-point contact. *Vehicle Syst. Dyn.* 43, 6-7 (2005), 455–483.
- [19] ROZENBLAT, G. *Dynamical Systems with Dry Friction*. NITs Regular and Chaotic Dynamics, Moscow-Izhevsk, 2006.

- [20] SILANTYEVA, O., AND DMITRIEV, N. Dynamics of bodies under symmetric and asymmetric orthotropic friction forces. In *Advances in Mechanics: Theoretical, Computational and Interdisciplinary Issues* (London, 2016), CRC Press/Balkema, Taylor & Francis Group, eds. M. Kleiber et al., pp. 511–515.
- [21] WEIDMAN, P., AND MALHOTRA, C. On the terminal motion of sliding spinning disks with uniform coulomb friction. *Phys. D* 233, 1 (2007), 1–13.
- [22] ZMITROWICZ, A. Mathematical descriptions of anisotropic friction. *Int.J.Solids Struct.* 25, 8 (1989), 837–862.
- [23] ZMITROWICZ, A. illustrative examples of centrosymmetric and non-centrosymmetric anisotropic friction. *Int.J.Solids Struct.* 29, 23 (1992), 3045–3059.
- [24] ZMITROWICZ, A. Models of kinematic dependent anisotropic and heterogeneous friction. *Int.J.Solids Struct.* 43 (2005), 4407–4451.
- [25] ZMITROWICZ, A. Contact stresses: a short survey of models and methods of computations. *Arch App Mech* 80 (2010), 1407–1428.